Journal of Magnetics 11(4), 195-207 (2006)

<Invited review paper>

Frontiers in Magneto-optics of Magnetophotonic Crystals

M. Inoue[1], A. A. Fedyanin[2]*, A. V. Baryshev[1,3], A. B. Khanikaev[1], H. Uchida[1], and A. B. Granovsky[2]

[1]*Toyohashi University of Technology, Toyohashi 441-8580, Japan*
[2]*Department of Physics, M.V. Lomonosov Moscow State University, 119992 Moscow, Russia*
[3]*Permanent address: Ioffe Physico-Technical Institute, 194021 St. Petersburg, Russia*

(Received 12 December 2006)

The recently published and new results on design and fabrication of magnetophotonic crystals of different dimensionality are surveyed. Coupling of polarized light to 3D photonic crystals based on synthetic opals was studied in the case of low dielectric contrast. Transmissivity of opals was demonstrated to strongly depend on the propagation direction of light and its polarization. It was shown that in a vicinity of the frequency of a single Bragg resonance in a 3D photonic crystal the incident linearly polarized light excites inside the crystal the TE- and TM-eigen modes which passing through the crystal is influenced by Bragg diffraction of electromagnetic field from different (hkl) sets of crystallographic planes. We also measured the Faraday effect of opals immersed in a magneto-optically active liquid. It was shown that the behavior of the Faraday rotation spectrum of the system of the opal sample and magneto-optically active liquid directly interrelates with transmittance anisotropy of the opal sample. The photonic band structure, transmittance and Faraday rotation of the light in three-dimensional magnetophotonic crystals of simple cubic and face centered cubic lattices formed from magneto-optically active spheres where studied by the layer Korringa-Kohn-Rostoker method. We found that a photonic band structure is most significantly altered by the magneto-optical activity of spheres for the high-symmetry directions where the degeneracies between TE and TM polarized modes for the corresponding non-magnetic photonic crystals exist. The significant enhancement of the Faraday rotation appears for these directions in the proximity of the band edges, because of the slowing down of the light. New approaches for one-dimensional magnetophotonic crystals fabrication optimized for the magneto-optical Faraday effect enhancement are proposed and realized. One-dimensional magnetophotonic crystals utilizing the second and the third photonic band gaps optimized for the Faraday effect enhancement have been successfully fabricated. Additionally, magnetophotonic crystals consist of a stack of ferrimagnetic Bi-substituted yttrium-iron garnet layers alternated with dielectric silicon oxide layers of the same optical thickness. High refractive index difference provides the strong spatial localization of the electromagnetic field with the wavelength corresponding to the long-wavelength edge of the photonic band gap.

Keywords : magneto-optics, photonic crystal, magnetophotonic, yttrium-rion garnet

1. Introduction

Lately, there has been much interest in a new class of artificial structures known as photonic crystals (PC's) owing to many different non-trivial electromagnetic effects that were predicted in PC's. The most advanced ideas are associated with a total inhibition of spontaneous emission [1] and a strong localization of light [2] when photons of certain energy cannot propagate through the structure along any direction and with any polarization. These effects can be observed in photonic materials with periodic 3D modulation of the dielectric constant. At present, there is much work on the study of the photonic gap energy with the light wavevector examined by angle-resolved reflection or transmission spectroscopy. However, there are only few reports on polarization-resolved study of 3D PC's [3-7] and, in fact, coupling of the polarized light to 3D PC's is not studied well up to now. Meanwhile, the nature of the polarized light coupling to PC's is of great importance for study on optical properties of magnetophotonic crystals (MPC's).

Recently, we reported that 1D MPC's composed of dielectric and magnetic materials exhibit remarkable magneto-optical (MO) properties accompanied by a huge augmentation in their Kerr and Faraday rotations [8], and a giant

*Corresponding author: Tel: +7-095-939-3669
Fax: +7-095-939-1104, e-mail: fedyanin@nanolab.phys.msu.ru

enhancement of the nonlinear magneto-optical response was observed [9]. There are only a few theoretical works devoted to 2D and 3D MPC's [10-13]. Experimental studies on fabrication, magnetic and optical properties of synthetic opal/magnetic material composites were reported in Refs. 14, 15. Studies on optical properties of 3D PC's based on synthetic opals in the case of low dielectric contrast [16] shows that synthetic opals have unique features to control visible light: they can diffract light selectively in 3D space, split a light beam into several beams and show a strong anisotropy in transmittance at the polarized light illumination. We consider 3D magnetophotonic crystals as more effective for applications. Since their photonic properties are sensitive to both magnetic and electric fields, they have the potential for use in a variety of optoelectronic devices. Among the progress in development two- and three-dimensional MPC's achieved last years the most advance is attained in the fabrication of 1D MPC's. In these multilayered structures the magnetic layer is sandwiched by a couple of dielectric Bragg reflectors and acts as a microcavity spacer provided a resonant microcavity mode at a certain wavelength inside PBG. Maximal transmittance and magneto-optical Faraday rotation is observed for the microcavity mode, when light of the resonant wavelength is localized in the magnetic layer. Additional growth of Faraday angle θ_F can be achieved by the increase of the spacer thickness or incorporation of the second magnetic spacers. However, the θ_F enhancement in these MPC's has a practical restriction stemming from the quality factor limited by the accuracy of the magnetic spacer thickness.

This Paper is organized as follows. In section II recent advances in magneto-optical studies of 3D MPC's are presented. Several aspects of calculation of magneto-optical response of 3D MPC's are discussed in Section III. Sections IV and V describe new approaches in fabrication of 1D MPC's with resonance enhancement of magneto-optical response in the high-order photonic band gap (PBG) and at the PBG edge. The results are summarized in Section VI.

2. Faraday effect and Bragg diffraction induced transmittance anisotropy in 3D opal photonic crystals

In this part the results of the study of polarized light coupling to oriented opal samples infiltrated with a liquid of close to silica refraction index both without and in presence of external magnetic field will be presented. We measured the polarization- and angle-resolved transmission spectra $T_k(\lambda)$ of opals and magneto-optical response of a

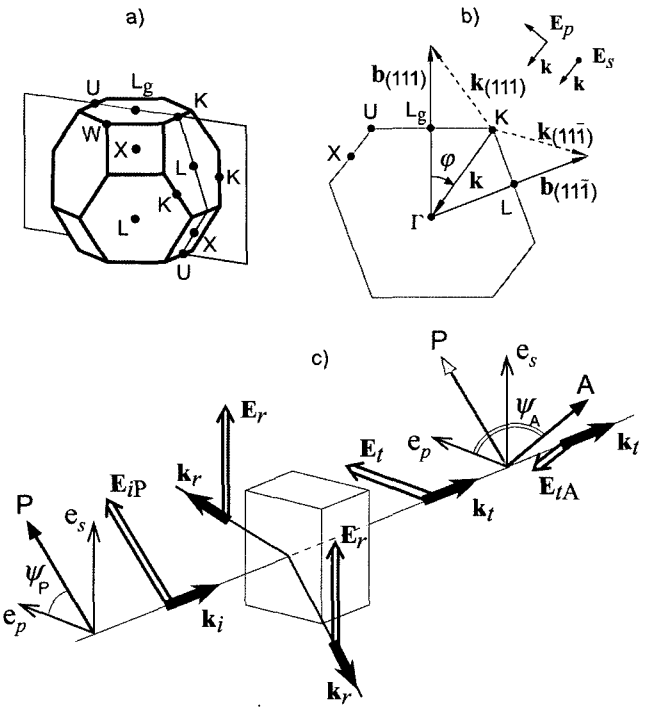

Fig. 1. (a) The BZ for the fcc crystal and the scanning plane, (b) the BZ cross-section and the $L_g \rightarrow K \rightarrow L$ scanning path, (c) schematic of experimental setup, illumination with the $\mathbf{E}_{45°}$-polarized light is presented.

system of opal sample and magneto-optically active liquid. High-quality synthetic opal sample [17] having the fcc structure was chosen for this study. The sample had the (111) growth surface of 10×10 mm^2 in size and about 1 mm in thickness, the diameter of SiO_2 spheres was 315 ± 15 nm. The selected diameter and $L_g \rightarrow K \rightarrow L$ scanning path [Fig. 1(a), (b)] allowed us to analyze the light coupling to the (111), ($\bar{1}$11), (020), (002) and (022) planes [18] in the spectral range of 365-825 nm (the L_g point corresponds to the growth direction [111]). The sample was placed between polarizer and analyzer, polarization azimuths of which can be changed from 0 to 360 degrees [Fig. 1(c)].

The transmission spectra of the sample were measured using a Shimadzu UV–3100 spectrophotometer. Transmittance was studied at different angles of incidence of light (φ) [Fig. 1(b)] and different azimuths of the polarizer (ψ_P) and analyzer (ψ_A) including configurations with the parallel ($\psi_P = \psi_A$) and mutually orthogonal azimuths ($\psi_P = \psi_A - 90°$). Angle-resolved transmission spectra were measured for three linear polarizations of the incident light beam: in plane ($\mathbf{E}_p$-polarization, $\psi_P = 0°$), normal ($\mathbf{E}_s$-polarization, $\psi_P = 90°$) and rotated through an angle of $\psi_P = 45°$ with respect to the L_gGL scanning plane [$\mathbf{E}_{45°}$-polarization, the case is shown in Fig. 1(c)].

Magneto-optical properties of the system of the opal sample and magneto-optically active liquid were studied with a setup to measure the Faraday effect. The setup consists of an optical bench where the light beam passes through the polarizer, electromagnet in which sample is placed into a vessel with an immersion magneto-active liquid, analyzer and detector. In our study, the sample was infiltrated with a transparent paramagnetic liquid, the saturated isopropyl-alcohol solution of dysprosium nitrate [IPA-$Dy(NO_3)_3$]. The linearly polarized electric field $\mathbf{E}_s$ was chosen to be perpendicular to the scanning plane $L_g\Gamma L$ [Fig. 1(a)]. Reversing magnetic field up to 2.3 kOe was applied along the light propagation direction. We measured rotation of the plane of polarization as a function of applied magnetic field when light beam propagates along the $\Gamma \rightarrow K$ direction in the sample. Figure 2 shows experimental data on the polarized light coupling to the sample under study: (a)-(d) graphs present the transmittance through the sample when polarizations of incident and measured light beams are preset to be parallel ($\psi_P=\psi_A$), (e)-(h) graphs plot the transmittance through the sample when measuring only the linearly independent polarization component ($\psi_P=\psi_A-90°$). Hereafter, we specify the following notations: $T_{s,s}$, $T_{p,p}$ and $T_{45°,45°}$ [the first (second) index is the azimuth of the polarizer (analyzer) with respect to the $L_g\Gamma L$ scanning plane] as the transmittance measured when azimuths of the polarizer and analyzer are parallel; $T_{s,p}$, $T_{p,s}$ and $T_{45°,135°}$ as the transmittance measured when azimuths are mutually orthogonal. Note that the $T_{s,s}$, $T_{p,p}$ and $T_{45°,45°}$ show the transmittance of light with the polarization chosen by the polarizer; the transmittance of light with linearly independent polarization, and thus the change in polarization, is manifested by the $T_{s,p}$, $T_{p,s}$ and $T_{45°,135°}$ spectra.

The $T_{s,s}$, $T_{p,p}$ and $T_{45°,45°}$ spectra shown in the (a)-(d) graphs manifest the φ-dependent intensive deeps, they undergo spectral shift in accordance with the Bragg law and symmetry of the fcc lattice. We have shown that the spectral positions of stop bands in spectra coincide well with the calculated variation of the Bragg wavelengths for the diffraction from the (*hkl*) planes [16]. The most pronounced deeps are found to be due to the {111} planes. At normal incidence onto the (111) plane ($\varphi = 0$), the $T_{s,s}$, $T_{p,p}$ and $T_{45°,45°}$ transmission spectra practically coincide [Fig. 2(a)] and show an intensive deep associated with the (111) stop band. In moving from the L_g point to the L point, the minimum of the (111) deep in the $T_{s,s}$ spectra shifts from $\lambda_{min}^{(111)} = 710$ nm at $\varphi = 0$ to the short wavelength range: 690 nm ($\varphi = 15°$), 620 nm ($\varphi = 35°$) and 530 nm ($\varphi = 45°$). As for the $(\bar{1}11)$ photonic stop band, the respective deep shows opposite shifts from about 450 nm at $\theta = 15°$ [Fig. 2(b)] to the value of about 590 nm at $\varphi = 35°$ and 650 nm at $\varphi = 45°$. Note that in the vicinity of the K point ($\varphi \approx 35°$) the deep in transmission spectra is a convergence of the (111) and $(\bar{1}11)$ photonic stop bands, and true positions of the related stop bands are difficult to evaluate. The mentioned shifts of stop bands and their convergence are found to be more obvious in the $T_{s,s}$ spectra. As for the $T_{p,p}$ and $T_{45°,45°}$ spectra, the shifts of the (111) and $(\bar{1}11)$ stop bands are well defined in the long wavelength range and masked in short wavelengths.

The features in transmission spectra taken for different polarizations at the same angles φ are recently reported [6]. It was shown that for opal photonic crystals at the condition of a small dielectric contrast, the features in the polarization-resolved transmission spectra can be coarsely understood in terms of the Fresnel theory and Brewster effect with the account of 3D structure of synthetic opals. In fact, the incident linearly polarized light probing a 3D PC splits into the TE- and TM-modes with respect to every (*hkl*) set of crystallographic planes existing in the crystal. Analyzing the φ-dependent wavevector components (k_x, k_y, k_z), orientation of the plane of polarization and

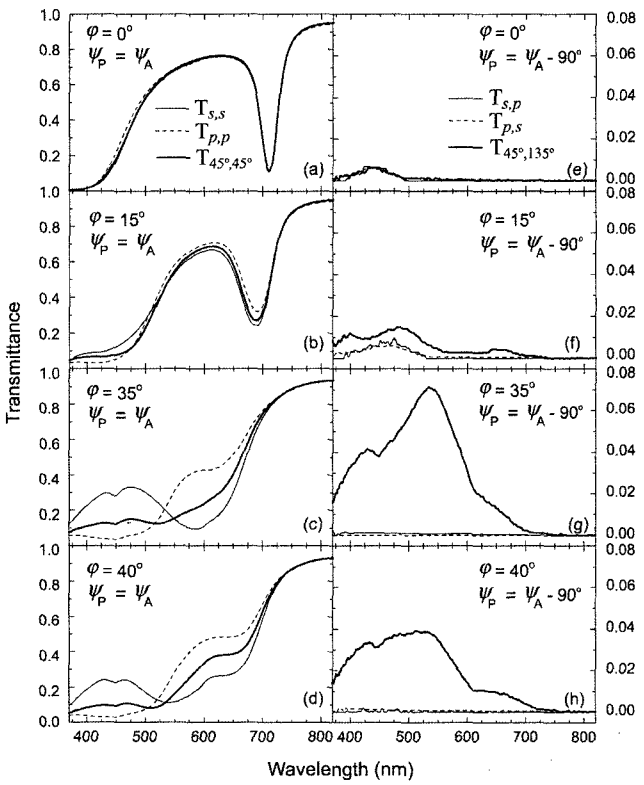

Fig. 2. Transmission spectra taken along the $L_g \rightarrow K \rightarrow L$ paths from an opal sample made up of ordered a-SiO_2 spheres with a diameter of 315 ± 15 nm. (a)-(d) graphs present the transmittance taken at azimuth of the polarizer and analyzer being parallel ($\psi_P=\psi_A$), (e)-(h) $-\psi_P=\psi_A-90°$.

Miller indices for the vector $\boldsymbol{n}_{(hkl)}$ normal to the (*hkl*) plane, we can determine two angles that are of our interest – the angle of incidence onto the (*hkl*) plane and angle between the plane of polarization and the vector $\boldsymbol{n}_{(hkl)}$. The pairs of these two angles for every set of crystallographic planes define transmittance of polarized light in 3D PC. It is worth mentioning that up to five Bragg resonances [(111), ($\bar{1}$11), (020), (002) and (022)] could be seen for the sample under study in the visible spectral range, and in general case the propagating light of a fixed wavelength is a mixture of the TE- and TM-modes.

Bragg resonance suppression effect is clearly seen in Fig. 2(b)-(d), it reveals itself as the appearance of critical angles of incidence for the TM-modes passing without Bragg reflection through the crystal planes. Spectra manifest that deeps corresponding to the (111) and ($\bar{1}$11) stop bands are intensive for the incident $\mathbf{E}_s$-polarized light, which is the TE-wave strongly diffracting from the (111) and ($\bar{1}$11) planes. While at illumination with the $\mathbf{E}_p$-polarized light, which is the TM-wave for the given planes, the (111) and ($\bar{1}$11) deeps are shallow. There is no clear appearance of the ($\bar{1}$11) stop band in the $T_{p,p}$ spectrum taken at $\varphi = 35°$ and of the (111) stop band in the $T_{p,p}$ spectrum taken at $\varphi = 40°$. As for the $T_{45°,45°}$ spectra, one can see that their shape is some averaging of intensities of stop bands in the $T_{s,s}$ and $T_{p,p}$ spectra. We see that the Bragg resonance suppression effect gives rise to the transmittance anisotropy of the photonic crystals and, as we show below, is responsible for the modification in polarization of transmitted light [Fig. 2(e)-(h)].

Let us analyze how polarization dependent Bragg diffraction of light from crystal planes act on the polarization of transmitted light. Figures 2(e)-(h) show the $T_{s,p}$, $T_{p,s}$ and $T_{45°,135°}$ transmittance for different angles of φ, when the polarizer and analyzer are crossed ($\psi_P = \psi_A - 90°$). We observe that the $T_{s,p}$ and $T_{p,s}$ transmittance are negligible in the spectral range where the (111) and ($\bar{1}$11) stop bands exist. What this means is that the plane of polarization of the TE- (or TM) mode passing the crystal is not changed, $\mathbf{E}_t = \mathbf{E}_s$ (or $\mathbf{E}_t = \mathbf{E}_p$). However, in contrast to the $T_{s,p}$ and $T_{p,s}$ cases the signal in the $T_{45°,135°}$ spectra rises significantly as the wavelength of the incident beam reaches photonic stop bands. This is thus a demonstration of a change in polarization state of transmitted light beam as shown in Fig. 1(c), which is found to be maximal at illumination with the $\mathbf{E}_{45°}$-polarized light along the G → K direction. Under such illumination the $\mathbf{E}_{45°}$-polarized incident wave splits into the TE- and TM- modes for the (111) and ($\bar{1}$11) planes. These modes pass the sample in the same direction with sufficiently different intensities and construct the resultant transmitted wave having dissimilar polarization, $\mathbf{E}_t \neq \mathbf{E}_{45°}$. Note that the Bragg resonant light propagating in the G → K direction couples simultaneously both the (111) and ($\bar{1}$11) sets of planes, that is why it experiences the maximum change in its polarization. It is obvious that for a single Bragg resonance, the change in polarization of the transmitted light reaches its maximum at a critical angle when the TM-mode propagates without reflection through the crystal, and the TE-mode is completely reflected due to Bragg diffraction. In the short wavelengths of about 400 nm one can see the rise of transmittance in the $T_{s,p}$ (and $T_{p,s}$) spectra [Fig. 2(e), (f)]. This rise has the discussed above nature and is explained by the transmittance anisotropy involving the (020), (002) and (022) planes.

Now we turn to study on magneto-optical response of the system of the opal sample and magneto-optically active liquid (Fig. 3). First, we measured Faraday rotation (θ_F) of the saturated isopropyl-alcohol solution of dysprosium nitrate (spectrum 1). Faraday rotation of the opal sample immersed in the IPA-$Dy(NO_3)_3$ solution was measured for the E_s-polarized beam passing the sample along the G → K direction (spectrum 2). For the spectral range of the (111) and ($\bar{1}$11) stop bands, spectrum 2 is defined by transmittance through the opal sample (spectrum 3), and outside the mentioned range spectrum 2 follows spectrum 1 of the IPA-$Dy(NO_3)_3$ solution.

Note that the IPA-$Dy(NO_3)_3$ solution shows negative rotation of plane of polarization, but in the presence of the opal sample rotation becomes positive for the Bragg resonant light. According to polarized light coupling in the case of the $\mathbf{E}_s$-illumination and when magnetic field is not applied, there is no TE-TM splitting of the incident

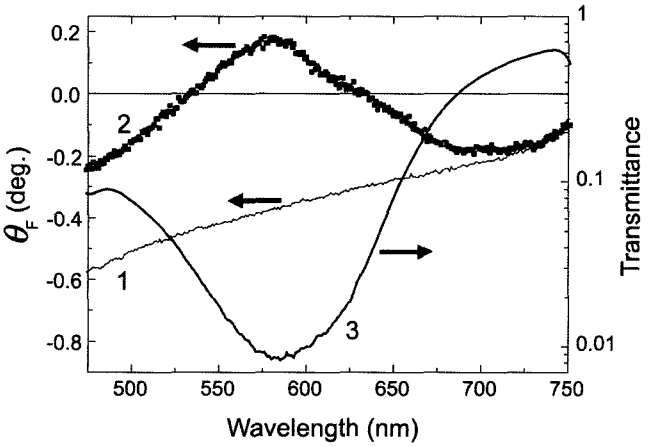

Fig. 3. (1) – Faraday rotation of the saturated isopropyl-alcohol solution of dysprosium nitrate [IPA-$Dy(NO_3)_3$]. (2) – Faraday rotation of the system of the opal sample and IPA-$Dy(NO_3)_3$ solution. (3) – transmissivity of the opal sample at illumination with the $\mathbf{E}_s$-polarized light.

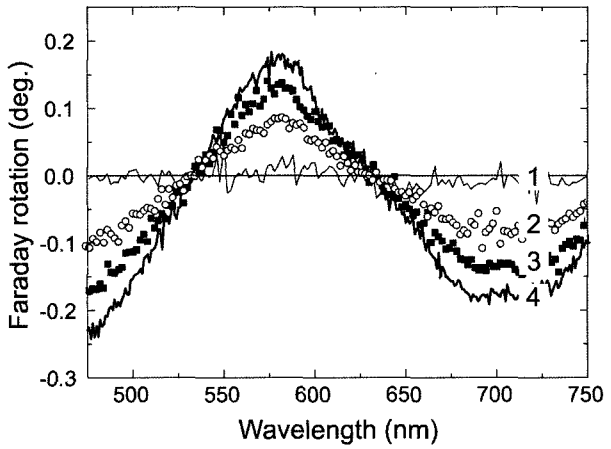

Fig. 4. Faraday rotation of the system of the opal sample immersed into IPA-Dy$(NO_3)_3$ solution. Spectra were taken at different magnitude of external magnetic field: (1) – H = 0 kOe, (2) – H = 1 kOe, (3) – H = 1.7 kOe, and (4) – H = 2.3 kOe.

light around the (111) and ($\bar{1}$11) Bragg resonances [see Fig. 2(g)]. However, if magnetic field (H) is applied, the $\mathbf{E}_s$- plane of polarization is rotated by the IPA-Dy$(NO_3)_3$ solution and there appears a wave which is incident on the opal sample and then splits into TE- and TM-components. Since the TE-mode experiences strong coupling to the opal sample in the vicinity of Bragg resonance (see spectrum 3, transmittance is of 0.01), the intensity of this mode decreases extremely and the orientation of the plane of polarization has to change significantly due to Bragg resonance suppression [see Fig. 2(e)-(h), $T_{45°,135°}$ spectra]. On the other hand the TE-mode scattering (both forward and back) in the crystal volume is stronger in comparison to TM-mode scattering. One should expect that θ_F which is accumulative in PC is largely defined by the TE-mode. Two mentioned above processes change orientation of plane of polarization when magnetic field is applied.

Thus, for the system of the opal sample and magneto-optically active liquid, we have two parameters to affect the polarization of transmitted wave: the degree of TE-TM splitting and the actual value of θ_F for the opal sample infiltrated with immersion liquid. Note that θ_F of synthetic opal itself is positive – a fused silica glass type, but the immersion liquid that is inside and outside the opal sample shows negative Faraday rotation (Fig. 3).

Figure 4 shows magneto-optical response of the system of the opal sample and magneto-optically active liquid at different magnitude of magnetic field (H). As it was expected for the $\mathbf{E}_s$-polarized light at H=0 kOe, transmitted wave has the same polarization as the incident wave, and the measured spectrum (curve 1) shows zero signal. It is observed that rotation of plane of polarization becomes more pronounced as the magnitude of magnetic field rises (curves 2-4), and θ_F reaches a maximum.

3. Calculations of Faraday effect in three-dimensional magnetophotonic crystals: the layer Korringa-Kohn-Rostoker method

In this part we extend the layer Korringa-Kohn-Rostoker (LKKR) method to study the photonic band structure (PBS) and the MO properties of the three-dimensional MPC's those consist of non-overlapping MO active spheres arranged periodically in an isotropic host material. Magnetization induced alteration of the PBS and transmission spectra of the MPC's with simple cubic and face centered cubic (fcc) lattices was studied. Finally, we analyzed MO properties of a magneto-photonic heterostructure – the three-dimensional PC with a planar magnetic defect.

The Korringa-Kohn-Rostoker (KKR) method as well as its modification for layered systems (LKKR) has been extensively and very successfully used in the study of the electronic structure and related electronic properties of various materials. Recently, several groups have also developed the KKR [19] and LKKR formalism for electromagnetic (EM) waves [20]. The advantage of the LKKR is that one can calculate the PBS together with transmissivity and reflectivity spectra, which can be directly compared with experimental data.

It is well-known that EM waves propagating along the magnetization direction in MO active medium characterized by permeability μ and the permittivity tensor

$$\hat{\varepsilon} = \begin{pmatrix} \varepsilon_{11} & i\varepsilon_{12} & 0 \\ -i\varepsilon_{12} & \varepsilon_{11} & 0 \\ 0 & 0 & \varepsilon_{11} \end{pmatrix} \tag{1}$$

are essentially the circularly polarized waves of left (L) or right (R) handedness. The associated wave numbers or the L and R waves are given by

$$k_{R,L} = \frac{\omega}{c}\sqrt{(\varepsilon_{11} \pm \varepsilon_{12})\mu}, \tag{2}$$

where $c = 1/\sqrt{\varepsilon_0\mu_0}$ is the velocity of light. Therefore, the polarization plane of the transmitted light, which emerges the slab of a MO material, will be rotated trough an angle θ_F called the Faraday rotation angle.

The LKKR formalism (as well as KKR) requires knowledge of the scattering properties of the elementary scatterer of the PC. Therefore, at the first stage, we need to deal with the scattering of an EM wave of wave number $k_b = \sqrt{\varepsilon_b\mu_b}\,\omega/c$ by a MO active sphere with permittivity tensor $\hat{\varepsilon}$, permeability μ and radius R, which is embedded

in a optically inactive isotropic host medium defined by ε_b and μ_b. Assuming an exi($-i\omega t$) time dependence we express the EM field outside the sphere as follows [20]:

$$\vec{E}(\vec{r}) = \vec{E}_{in}(\vec{r}) + \vec{E}_{sc}(\vec{r}) =$$

$$\sum_{l,m} \left\{ \left[a_{lm}^{0E} \frac{i}{k_b} \nabla \times j_l(k_b r) \mathbf{X}_{lm}(\mathbf{r}) + a_{lm}^{0H} j_l(k_b r) \mathbf{X}_{lm}(\mathbf{r}) \right] + , \right.$$

$$\left. + \left[a_{lm}^{+E} \frac{i}{k_b} \nabla \times h_l^+(k_b r) \mathbf{X}_{lm}(\mathbf{r}) + a_{lm}^{+H} h_l^+(k_b r) \mathbf{X}_{lm}(\mathbf{r}) \right] \right\} \quad (3)$$

where j_l and h_l^+ are spherical Bessel and Hankel functions, respectively, and $\mathbf{X}_{lm}(\hat{\mathbf{r}})$ are vector spherical harmonics. The coefficients a_{lm}^{0E} and a_{lm}^{0H} refer to the incident wave, whereas a_{lm}^{+E} and a_{lm}^{+H} to the scattered wave. These coefficients are related to the scattering matrix as follows:

$$a_{lm}^{+P} = \sum_{l',m',P'} T_{lm,l',m'}^{PP'} a_{l',m'}^{0P'}., \quad (4)$$

where $P=(E, H)$. We assumed in our calculations that $\mu_b=\mu=1$. With this assumption and using the exact solution of the EM field inside a MO active sphere [21] we can find the scattering matrix $T_{lm,l',m'}^{PP'}$.

Although the KKR formalism can deal with situations in which the parameters of the problem depend on the frequency, in our calculations, for simplicity and to do not obscure the main effects of the MO activity, we assumed that $\hat{\varepsilon}$ and μ are constant over the considered frequency range.

We examined photonic crystals with the sc (and fcc) lattice of nonoverlapping spheres (one sphere per lattice site, the lattice constant a_0; in the case of sc lattice the slab under study was made as a sequence of the (001) planes, and for the fcc lattice – (111) planes. Having obtained the scattering matrix for a single MO active sphere, we can apply LKKR technique to calculate the PBS and the transmittance of slabs-[20].

The first question we have to answer is how the MO activity of the spheres affects the PBS of magnetophotonic crystals. Figs. 5 and 6 show sections of the PBS of sc and fcc photonic crystals along the normal to the (001) and (111) planes, respectively. Direction of light propagation and the magnetization direction in slabs coincide with to the ΓX (for the sc lattice) and ΓL (for the fcc lattice) high-symmetry directions. We found that, when MO activity is present, the degenerate *s*- and *p*-polarized bands of the non-magnetic crystal split into two bands. These bands correspond to the circularly polarized light of *R* and *L* handedness.

Apart from this splitting of the bands, the changes in the dispersion curves and transmission spectra brought about by the MO activity of the spheres are marginal. At the same time our results show that the band structure of MPC is richer than that obtained in PCs composed of

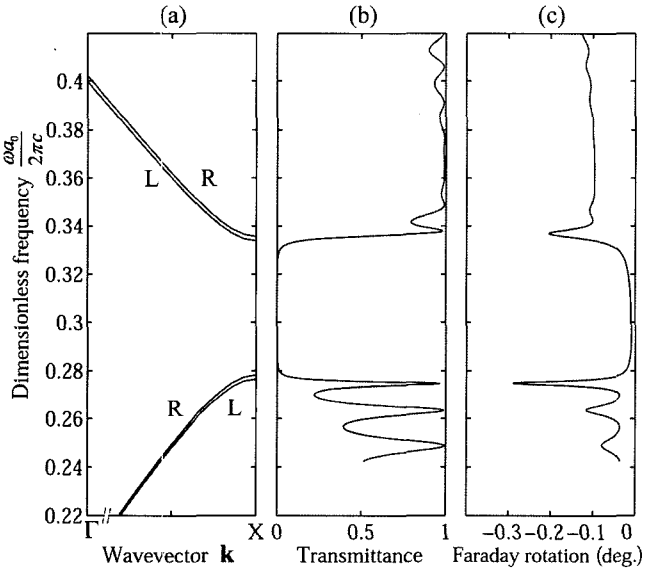

Fig. 5. (a) Band structure for the EM field along the normal to the (001) surface of a simple cubic photonic crystal. The photonic crystal consists of MO spheres with $\varepsilon_{11}=5.59$, $\varepsilon_{12}=-3.69\times10^{-3}$ and $R_s/a_0=0.5$ radius in the air background. The transmittance (b) and Faraday rotation (c) were calculated for normal incidence of light onto a slab composed of 16 layers of the (001) planes of MO spheres with $\varepsilon_{11}=5.59+i5.42\times10^{-3}$, $\varepsilon_{12}=-3.69\times10^{-3}$ (Bi:YIG at 700 nm) and radius $R_s/a_0=0.5$ in the air background.

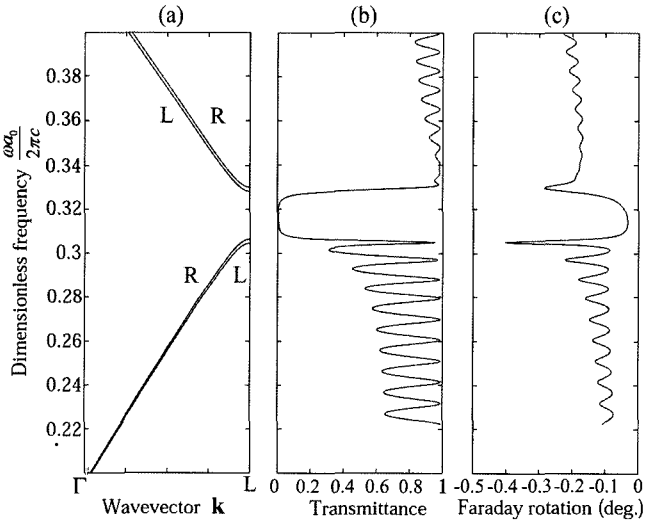

Fig. 6. (a) Band structure for the EM field along the normal to the (111) surface of a fcc crystal. The crystal consists of MO spheres with the same parameters as for Fig. 1a. The transmittance (b) and Faraday rotation (c) were calculated for normal incidence of light onto a slab composed of 16 layers of the (111) planes of MO spheres with the same parameters as for Figs. 1b-c.

nonmagnetic isotropic spheres because of reduction of the crystal symmetry by MO activity.

Although the MO activity of the spheres does not affect significantly the PBS and transmission spectra of the crystals, it renders crystal to be MO active, as shown in the Figs. 5(c)c and 6c. A linearly polarized plane wave incident normally on a slab of the crystal excites the two Bloch waves, denoted by R and L, which propagate through the slab with different phase velocities; transmission spectra are given in Figs. 5(b) and 6(b). If, as it appears to be the case, except the small frequency range in the proximity of the band edges, the R and L components of the transmitted wave have the same amplitude, the transmitted wave will be the linearly polarized one with the plane of polarization turned by an angle

$$\theta_F(\omega) \approx \frac{[k_z^R(\omega) - k_z^L(\omega)]}{2} d. \quad (6)$$

The oscillations in the Faraday rotation and transmission spectra are the result of the interference between waves reflected forward and backward at the two surfaces of the slab.

The value of the of the Faraday rotation angle of the finite slabs of PCs calculated by LKKR (Figs. 5(c) and 6c) is in the good agreement with that deduced from Eq. 6 and band structure of the infinite crystals shown in Figs. 5a and 6a, even when absorption by the MO spheres in the slabs in the calculations of the transmission spectra is taken into account. Therefore, we conclude that rotary power of the MPC's can be readily evaluated with a reasonably high precision.

It is worth pointing out that the Faraday rotary power of the crystals significantly increases at the band edges. This is what one expects because of slowing down of the EM waves at the band edges and cumulative character of the Faraday effect, these features result in the increasing of the difference between phase velocities of the R and L waves and, according to (6), the rise of the Faraday rotation. We also note that only the R (L) waves exist in a frequency range near lower (upper) band edge, which means that an incident linearly polarized light within this frequency range will emerge from the slabs as the left-hand (right-hand) circularly polarized wave. If we consider slabs of the PCs composed of positively rotating MO spheres, i.e. with non-diagonal element of the permittivity tensor ε_{12} of the opposite sign to that used in the present numerical simulation, or change magnetization direction to the opposite, handedness of the transmitted waves would be reversed.

Finally we considered a magnetophotonic heterostructure consisted of MO defect layer sandwiched in between fcc PC slabs composed of the silica spheres in the air.

It seems to be instructive to make consideration of the properties of the 3D magnetophotonic heterostructures in the qualitative comparison with its 1D counterpart, namely, the MO defect incorporated into the 1D PC. Our study on the 3D PC heterostructures revealed inapplicability of the simple relation for the resonant transmission wavelength λ_0 usable for 1D structures:

$$m\lambda_0 = 2nd, \quad (7)$$

where m=1, 2, 3... is the positive integer, n is refractive index of the defect and d is its thickness. This expression is based on the phase difference gained by the wave during its propagation through the defect layer. However, in the 3D heterostructures complicated light scattering at the interfaces between the 3D PCs and defect layer results in impossibility to find any analytical expression similar to (7). Therefore the problem in the 3D case can be treated only numerically.

Fig. 7 shows the transmission and Faraday rotation spectra of the heterostructure under study. In analogy with 1D magnetophotonic crystals, the strong enhancement of the Faraday rotation appears at the resonance transmission and in its proximity. However, because of the lower quality factor for the defect mode in the 3D case, values of the Faraday rotation angle are significantly smaller than in similar 1D MPC's.

To summarize this Section, we extended the LKKR method to the case of MPC's and examined their photonic

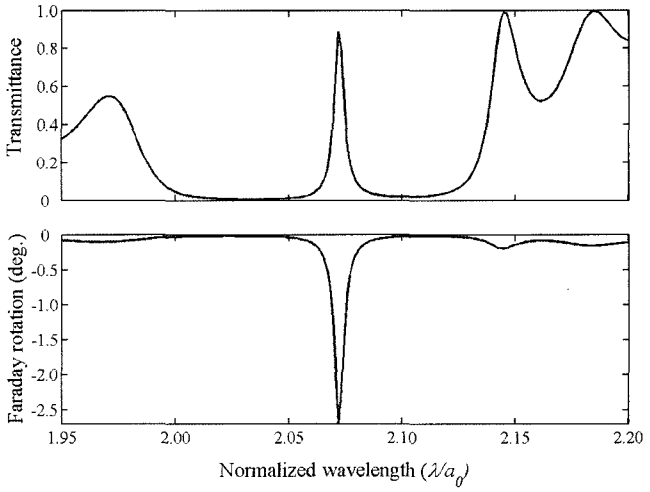

Fig. 7. Transmittance and Faraday rotation for the normal incidence on a heterostructure composed of the Bi:YIG layer sandwiched in between by fcc PC slabs. The thickness of the defect layer is d/a_0=0.56 while the permittivity is the same as for calculations presented in Figs. 1b-c. Each PC slab consists of 24 planes of close packed silica spheres in the air; these (111) planes are parallel to the basal surface of the slab.

band structure, transmittance and Faraday rotation spectra. Calculations were made for slabs of MPC's with simple cubic and face-centered cubic lattices composed of non-overlapping MO active spheres in air.

It was shown that for high-symmetry directions the MO activity reduces the symmetry of MPC's and leads to the splitting of branches of PBS, which are degenerate in the corresponding non-magnetic crystals. The polarization state of the eigenmodes corresponding to these branches changes from the linear *s* and *p* polarization to the circular polarization of the left and right handedness, and calculations show strong enhancement of the Faraday rotation. The latter fact reflects significant difference in the phase velocities of the *R* and *L* waves due to slowdown of EM waves, when approaching the bang edges, and the cumulative and/or non-reciprocal nature of the Faraday effect. For directions different from the high symmetry directions, when branches in the PBS of the corresponding non-magnetic PC are non-degenerate, the influence of the MO activity is negligible and polarization state of eigenmodes remains unaltered. In this case calculations demonstrate suppression and vanishing of the Faraday rotation.

4. The 1D MPC Utilizing the Second Photonic Band Gap

We fabricated a new one-dimensional magnetophotonic crystal utilizing the second and third photonic band gaps. Transmission spectrum of this 1D MPC has not only the first PBG that is located at designed spectral range, but also many high order PBGs in short wavelength region. Since the spectral distance between high order PBGs is shorter than one between the first and the second PBGs, the 1D-MPC with high order PBGs can be applied to a photonic band pass filter, and so on. Furthermore, use of the high order PBGs in the MPC with the large periodicity may be one of solutions for fabrication of 2D- and 3D-MPC's with high-quality structure. Until now, linear and nonlinear magneto-optical properties of the 1D-MPC's had been investigated for the first PBG, however, high order PBGs of the 1D-MPC's have not been discussed yet. Then we studied the 1D-MPC utilizing the second and the third PBGs to clarify their optical and magneto-optical properties.

Structure of the 1D-MPC is $(Ta_2O_5/SiO_2)^5$/Bi:YIG/$(SiO_2/Ta_2O_5)^5$ formed on a fused quartz substrate. Wavelength λ at a localized mode in the second PBG was designed to be 900 nm. Optical length of Ta_2O_5 and SiO_2 was $3\lambda/4$; one of Bi:YIG was $\lambda/2$. Difference from the 1D-MPC utilizing the first PBG is optical lengths of Ta_2O_5 and SiO_2, whose length are $\lambda/4$. Parameters of the designed

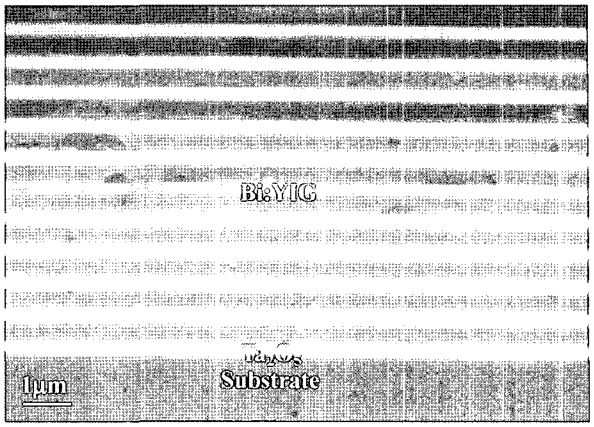

Fig. 8. SEM image of cross-section of the 1D-MPC having a localized mode in the second PBG around 900 nm.

structure were as follows: refractive index $n_{Ta_2O_5}$ is 2.05, thickness $d_{Ta_2O_5}$ is 329 nm; n_{SiO_2}=1.45, d_{SiO_2}=466 nm; $n_{Bi:YIG}$=2.36, $d_{Bi:YIG}$=191 nm. First, five pairs of the dielectric layers of Ta_2O_5 and SiO_2, the first Bragg reflector, were deposited on the fused quartz substrate by RF magnetron sputtering method. A Bi:YIG defect layer was also deposited on a top of the dielectric layers by RF magnetron sputtering method and was annealed in air at 700 °C for 15 minutes for crystallization of the magnetic garnet. Five pairs of dielectric films, the second Bragg reflector, were subsequently deposited.

Fig. 8 shows a cross-section of the fabricated 1D-MPC with a localized mode in the second PBG around 900 nm. Film thicknesses measured by FE-SEM were 307 nm for Ta_2O_5 and 454 nm for SiO_2 on average, and 260 nm for Bi:YIG. Because our RF magnetron sputtering system does not have monitoring system of film thickness during deposition, each film thickness of the 1D-MPC was not exactly equal to designed one. In the fabricated 1D-MPC,

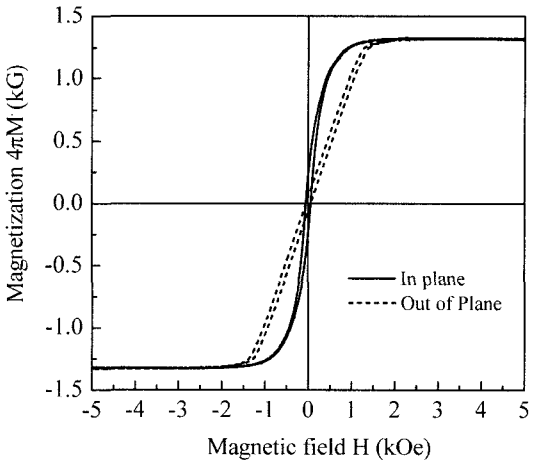

Fig. 9. Magnetization of a 1D-MPC.

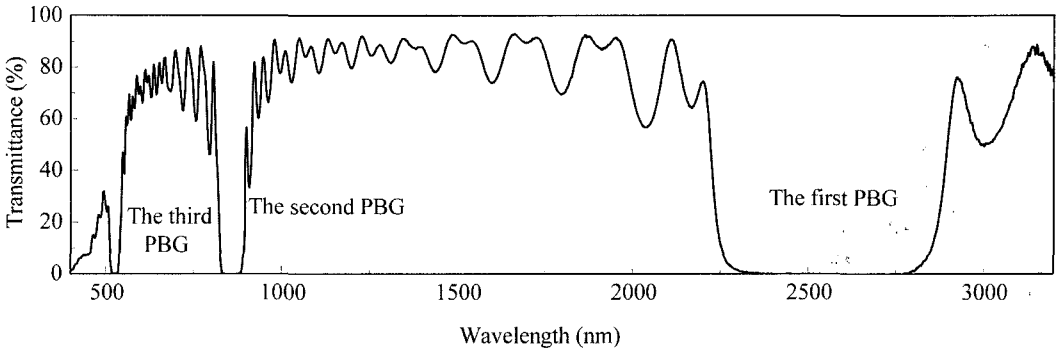

Fig. 10. Transmittance spectrum of the fabricated 1D-MPC having high order PBGs. Three PBGs exist in the wavelength region.

the saturation magnetization was about 1.3 kG (Fig. 9); the saturation magnetic field for the out-of-plane geometry was 1.5 kOe, which corresponds to Faraday configuration. In this measurement for Faraday rotation angle, magnetic field of 3 kOe was applied, which is larger than the saturation magnetic field.

Fig. 10 shows transmittance spectrum of the fabricated 1D-MPC having high order PBGs; the first PBG was located between 2200 and 2900 nm, the second PBG was between 820 and 930 nm, the third PBG was around 550 nm and the localized mode in the second PBG was at 894 nm. Since film thicknesses were different from the designed thicknesses, wavelength of the localized mode in the second PBG was shifted from 900 nm to 894 nm, and the center of the second PBG was also shifted to 860 nm. As seen in Fig. 10, the transmittance near the edge of the third PBG around 400 nm decreased drastically. This is the reason that the light of wavelength shorter than 600 nm was absorbed in the Bi:YIG defect layer, which can be understand by transmittance of single B:YIG film shown in Fig. 11(a).

The Bi:YIG is well known to be a magnetic material with high transparency [Fig. 11(a)]; maximum Faraday rotation occurs at 520 nm (Fig. 11(b)). Using the Bi:YIG as the defect layer of the 1D-MPC, enhancement of Faraday rotation was obtained at the localized mode in the first PBG. Fig. 12 shows experimental and computational magnified spectra including the second PBG and the third

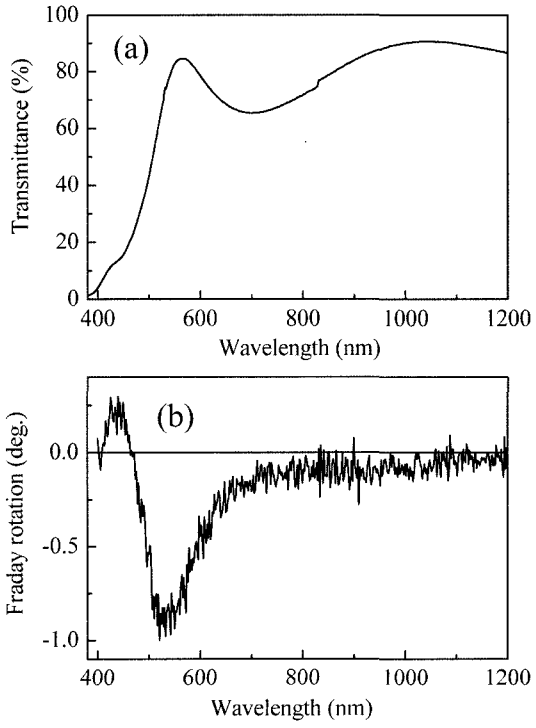

Fig. 11. (a) Transmittance and (b) Faraday rotation spectra of single Bi:YIG thin film with thickness of 250 nm.

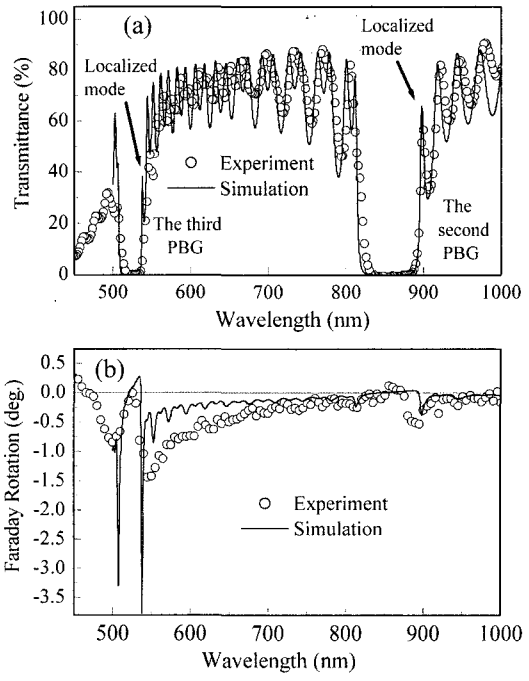

Fig. 12. Magnified spectra for (a) transmittance and (b) Faraday rotation of the 1D-MPC around the second and the third PBGs. Experimental data is denoted by open circle and calculated data is denoted by solid line.

PBG for (a) transmittance and (b) Faraday rotation. In the calculations, we used 4×4 matrix method; the film thicknesses measured by FE-SEM were used. As seen in Fig. 12, at the localized mode around 900 nm in the second PBG, transmittance of 57% was obtained (Fig. 12(a)), and enhancement of Faraday rotation angle of –0.5 degree was observed (Fig. 12(b)). In addition, at a localized mode in the third PBG vicinity of 540 nm, transmittance of about 30% and Faraday rotation angle of –1.5 degree were obtained. These angles are larger than the Faraday rotation of –0.2 degree (900 nm) and –0.8 degree (540 nm) for the single Bi:YIG film. Faraday rotation is enhanced by increment of effective optical thickness of Bi:YIG, which is induced by light interference in the periodic structure. As shown in Fig. 12, features of experimental spectra of transmittance and Faraday rotation (open circles) are in good agreement with the calculated spectra (solid lines).

However, Faraday rotation angles obtained by experiment and calculation were not the same magnitude as we expected before. It can be caused by shift of localized mode from center of the second PBG; therefore, accurate periodic structure is of importance to obtain large Faraday rotation in the 1D-MPC. Moreover, Faraday rotation angle at the localized mode in the second PBG was not large in comparison with the 1D-MPC utilizing the first PBG (the first PBG-MPC). In the second PBG-MPC with the localized mode at 900 nm in the second PBG, optical length of the Bi:YIG defect layer is same to the first PBG-MPC. However, optical lengths of dielectric layers of $3\lambda/4$ for the second PBG-MPC is thicker than one of $\lambda/4$ for the first PBG-MPC. Because extinction coefficient of Ta_2O_5 is not small, absorption of light is large in the second PBG-MPC with thick Ta_2O_5 layers. Therefore, reflection effect and light localization in the Bi:YIG defect layer of the second PBG-MPC might be small. If we use other dielectric material with small extinction coefficient, large Faraday rotation might be obtained at the localized mode in the second PGB. Otherwise, thin Ta_2O_5 layers in the periodic structure of the second PBG-MPC may be effective.

5. Faraday Rotation at Photonic-Band-Gap Edge in Garnet-Based Magnetophotonic Crystals

In this part another approach for the realization of the magneto-optical Faraday effect enhancement in 1D MPC's is discussed. It utilizes the spatial localization of light of the wavelength corresponding to the PBG edge. The θ_F growth is achieved by the combination of the field localization in many magnetic layers and the increase of the total magnetic material thickness [22, 23]. The idea is illustrated in Fig. 1a, where the dispersion relations $\omega(\mathbf{k}_L)$ and $\omega(\mathbf{k}_R)$ calculated for the left- and right-circular polarized optical waves propagating in a MPC formed from a stack of magnetic and nonmagnetic quarter-wavelength-thick layers are shown.

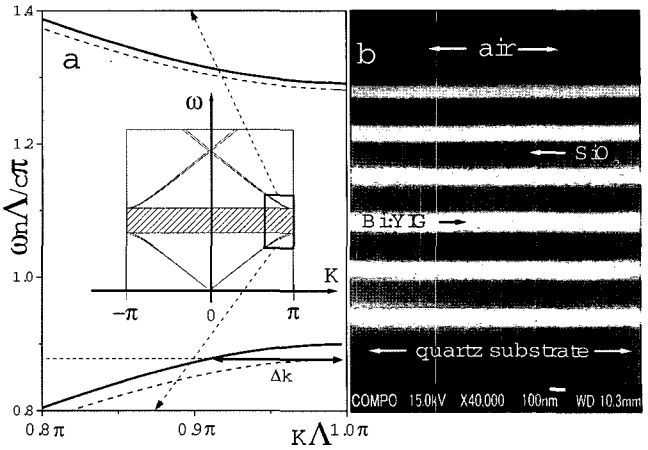

Fig. 13. (a). Band structure of an 1D MPC for the circular-polarized waves calculated for normal incidence onto the 1D MPC consisted of layers of nonmagnetic material with dielectric constant of ε_1=2.1 and magnetic one with diagonal component of dielectric constant of ε_2=5.6 and off-diagonal component (gyration) of g_2=–0.1i. (b). FESEM image of cleavage of the MPC under study The topmost and bottom-most layers are Bi:YIG films.

As $\mathbf{k}_L$ and $\mathbf{k}_R$ approach the boundary of the Brillouin zone at the long-wavelength PBG edge, dispersion curves flatten. This indicates decrease of group velocity v_g or slowing down the electromagnetic energy propagation velocity which relates directly to the spatial localization of light inside MPC. However, wave vectors $\mathbf{k}_L$ and $\mathbf{k}_R$ corresponding to the same frequency at the PBG edge differs significantly. This is a finger-print of the high effective circular birefringence and enhancement of magneto-optical Faraday rotation expected as the optical wavelength is tuned across PBG edge.

The pair of materials, bismuth-substituted yttrium-iron-garnet and silicon dioxide, is chosen for fabrication of 1D MPC's. Bi:YIG combines large Faraday rotation with low optical losses in red and infrared spectral region. MPC's are consisted of stack of alternating quarter-wave-thick ($\lambda_0/4$) layers of amorphous silicon dioxide and microcrystalline Bi:YIG, which were RF-sputtered onto the fused quartz substrate and annealed for Bi:YIG crystallization. A 2.5-mm thick fused quartz disk is used as a substrate which is called to resist to high lateral tensions in garnet layers during the multiple high temperature annealing of

the sample. After preparation of each successive garnet layer, the sample was removed from the sputtering machine and annealed in air at 700°C. Structure of the fabricated MPC was examined using the field-emission scanning electron microscope (FESEM) and atomic force microscope (AFM). The cleavage of the MPC is depicted in Fig. 13(b) and shows abrupt interfaces between magnetic garnet and dielectric layers as well as reproducible layer thickness in all repeats.

The AFM image of the MPC surface shows that Bi:YIG layers are formed from columnar microcrystals with lateral size from 1 to 2 μm. The roughness of approximately 2 nm was observed all over the garnet film surface; note that it was of 5 nm at the boundaries the film. Magnetic properties of MPC were studied using a vibrating-sample magnetometer. Hysteresis loop of the MPC at magnetic field applied along the normal to MPC (polar configuration) is shown in Fig. 14(b). Coercivity of the MPC in the polar configuration is estimated to be approximately 50 Oe and saturating magnetic field strength is close to 1.5~kOe. Large values of saturating field is attributed to the small Bi:YIG thickness, the easy-magnetization axis is shown to be directed along the layers with saturating field strength in the lateral configuration below 100 Oe.

Optical and magneto-optical spectra are shown in Fig. 15. The spectral range from 725 to 1025 nm where transmission is strongly suppressed corresponds to photonic band gap of the MPC. The Faraday rotation angle is also decreased in this spectral region. Outside PBG transmission is increased and shows interference fringes. The Faraday rotation angle θ_F also oscillates with spectrum having the local maxima at 640 and 720 nm correlating well with local transmission maxima. The largest enhancement of θ_F is observed near 1070 nm that coincides with the long-wavelength PBG edge. The spectrum of Faraday angle for an uniform slab of Bi:YIG with the

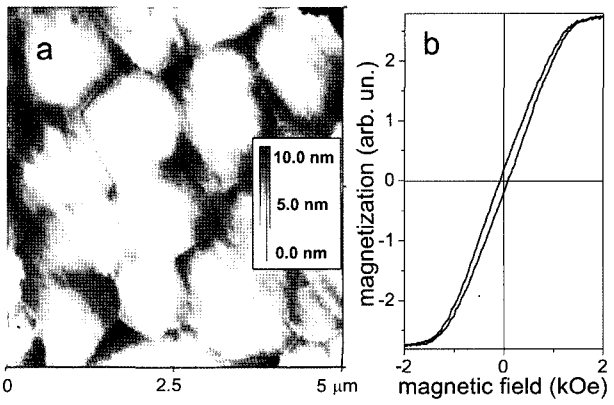

Fig. 14. (a). AFM image of the surface of the MPC studied. (b) The VSM data for polar configuration.

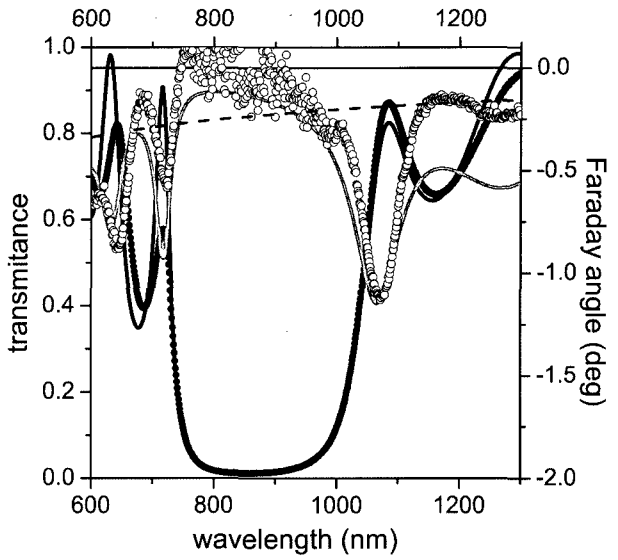

Fig. 15. The transmission spectrum of 1D MPC upon the normal incidence (filled circles). Faraday rotation angle spectrum (open circles). Solid curves are the fit to the data by the 4×4 matrix formalism. Dash curve is the interference-subtracted spectrum of Faraday angle in an homogeneous Bi:YIG slab of the same thickness.

thickness of 520 nm corresponding to the total Bi:YIG thickness in the MPC is calculated using the known spectra of diagonal and off-diagonal components of the complex dielectric function tensor of Bi:YIG with the same Bi concentration. The θ_F enhancement at the long-wavelength PBG edge reaches the value of 6.3 in comparison with homogeneous Bi:YIG slab while the rotation enhancement at the short-wavelength edge appear to be 1.9 and 2.7.

Both experimental spectra are fitted using the four-by-four matrix technique with spectral dependence of refractive indices and absorption coefficients are taken into account. The enhancement is predicted and experimentally observed at the wavelength tuned at the long-wavelength PBG edge at 1060 nm. The Faraday effect is 6.5 times enhanced in comparison with single Bi:YIG layer with the thickness equal to the total thickness of the magnetic material in the MPC. Experimental results are in good agreement with theoretical calculations. The correlation of θ_F and transmittance maxima opens up prospects for practical application of MPC in various magneto-optical devices as it gives an opportunity to rotate polarization plane without distortion or weakening transmitted light. The calculations also show that ellipticity of the transmitted light achieves minimum at the maximum of θ_F. Increasing the number of layers in MPC one can obtain better field localization combined with the total magnetic material thickness increase. Such combination is

expected to lead to significant θ_F dependence upon the number of layers (N) of MPC, i.e. its thickness.

6. Conclusions

In this paper recent achievements in design and fabrication, as well as in observation of MO response enhancement in different types of magnetophotonic crystals are presented. We report a study on the transmittance of linearly polarized light and change of its polarization for light beams propagating the opal photonic crystal. By applying magnetic field to the system of the opal sample and magneto-optically active liquid, the linearly polarized light beam passing the system changes its polarization. Rotation of the plane of polarization is found to be dependent on the magnitude of the applied magnetic field. It is shown that observed features in transmission spectra and magneto-optical response are due to the specific conditions for Bragg resonant light scattering on the families of crystal planes. We note that degree of TE-TM splitting and Faraday rotation in magnetophotonic photonic crystals influence simultaneously the detected rotation of the plane of polarization. With further understanding, these results serve as a basis for comprehensive evaluation of magneto-optical properties of 3D MPC.

We extended the LKKR method to the case of MPC's and examined the photonic band structure, transmittance and Faraday rotation spectra in simple cubic and fcc PCs slabs that consist of non-overlapping MO active spheres arranged periodically in an isotropic host medium. We found that a photonic band structure is most significantly altered by the magneto-optical activity of spheres for the high-symmetry directions where the degeneracies between the s- and p-polarized modes for the corresponding non-magnetic photonic crystals exist. The significant enhancement of the Faraday rotation appears for these directions in the proximity of the band edges, because of the slowing down of the light. While in the general case, when directions of incidence differ from these high-symmetry directions the Faraday rotation is suppressed.

New approaches for one-dimensional magnetophotonic crystals fabrication optimized for the magneto-optical Faraday effect enhancement is proposed and realized. First, we studied the 1D MPC utilizing the second and the third PBGs to clarify their optical and magneto-optical properties. Then, MPC's consist of a stack of ferrimagnetic Bi-substituted yttrium-iron garnet layers alternated with dielectric silicon oxide layers of the same optical thickness. High refractive index contrast provides the strong spatial localization of the electromagnetic field with the wavelength corresponding to the long-wavelength edge of the photonic band gap.

Acknowledgements

This work was supported by Giant-in-Aid (S) (No. 17106004.) from the Ministry of Education, Culture, Sport and Technology of Japan.

References

[1] E. Yablonovitch, Phys. Rev. Lett. **58**, 2059 (1987).
[2] S. John, Phys. Rev. Lett. **58**, 2486 (1987).
[3] I. I. Tarhan and G. H. Watson, Phys. Rev. Lett. **76**, 315 (1996).
[4] H. M. van Driel and W. L. Vos, Phys. Rev. B **62**, 9872 (2000).
[5] J. F. Galisteo-Lopez, F. Lopez-Tejeira, S. Rubio, C. Lopez, and J. Sanchez-Dehesa, Appl. Phys. Lett. **82**, 4068 (2003).
[6] A. V. Baryshev, A. B. Khanikaev, H. Uchida, M. Inoue, and M. F. Limonov, Phys. Rev. B **73**, 033103 (2006).
[7] M. V. Rybin, A. V. Baryshev, M. Inoue, A. A. Kaplyanskii, V. A. Kosobukin, M. F. Limonov, A. K. Samusev, A. V. Sel'kin, Photonics and Nanostructures–Fundamentals and Applications **4**, 146 (2006).
[8] M. Inoue and T. Fujii, J. Appl. Phys. **81**, 8 (1997). M. Inoue, K. I. Arai, T. Fujii, and M. Abe, J. Appl. Phys. **85**, 8 (1999). M. Inoue, K. I. Arai, T. Fujii, and M. Abe, J. Appl. Phys. **83**, 6768 (1998). M. Inoue *et al.*, J. Appl. Phys. **85**, 5768 (1999).
[9] A. A. Fedyanin, T. Yoshida, K. Nishimura, G. Marowsky, M. Inoue, and O. A. Aktsipetrov, JETP Lett. **76**, 527 (2002). T. V. Dolgova, A. A. Fedyanin, O. A. Aktsipetrov, K. Nishimura, H. Uchida, and M. Inoue, J. Appl. Phys. **95**, 7330 (2004). T. V. Murzina, R. V. Kapra, T. V. Dolgova, A. A. Fedyanin, O. A. Aktsipetrov, K. Nishimura, H. Uchida, and M. Inoue, Phys. Rev. B **70**, 012407 (2004).
[10] H. Nishizava and T. Nakayama, J. Phys. Soc. Jpn. **66**, 613 (1997).
[11] A. K. Zvezdin and V. I. Belotelov, Eur. Phys. J. B **37**, 479 (2004); V. Belotelov and A. Zvezdin, J. Opt. Soc. Am. B **22**, 286-292 (2005).
[12] A. B. Khanikaev, A. V. Baryshev, M. Inoue, A. B. Granovsky, and A. P. Vinogradov, Phys. Rev. B **72**, 035123 (2005).
[13] A. M. Merzlikin, A. P. Vinogradov, M. Inoue, and A. B. Granovsky, Phys. Rev. E **72**, 046603 (2005).
[14] C. Koerdt, G. L. J. A. Rikken, and E. P. Petrov, Appl. Phys. Lett. **82**, 1538 (2003).
[15] A. V. Baryshev, T. Kodama, K. Nishimura, H. Uchida, and M. Inoue, J. Appl. Phys. **95**, 7336 (2004); A. V. Baryshev, T. Kodama, K. Nishimura, H. Uchida, and M. Inoue, IEEE trans. Magn. **40**, 2829 (2004); T. Kodama, K. Nishimura, A. Baryshev, H. Uchida, M. Inoue, Phys. Stat. Sol. B **241**, 1597 (2004).

[16] A. V. Baryshev, A.V. Ankudinov, A. A. Kaplyanskii, V. A. Kosobukin, M. F. Limonov, K. B. Samusev, and D. E. Usvyat, Phys. Solid Slate **44**, 1648 (2002); A. V. Baryshev, A. A. Kaplyanskii, V. A. Kosobukin, M. F. Limonov, K. B. Samusev, and D. E. Usvyat, Phys. Solid Slate **45**, 459 (2003). A. V. Baryshev, A. A. Kaplyanskii, V. A. Kosobukin, M. F. Limonov, and A. P. Skvortsov, Phys. Solid Slate **46**, 1331 (2004). A. V. Baryshev, A. A. Kaplyanskii, V. A. Kosobukin, K. B. Samusev, D. E. Usvyat, and M. F. Limonov, Phys. Rev. B **70**, 113104 (2004); A. V. Baryshev, V. A. Kosobukin, K. B. Samusev, D. E. Usvyat, and M. F. Limonov, Phys. Rev. B **73**, 205118 (2006).

[17] Samples were purchased from "Opalon" Company, Moscow, Russia.

[18] Basically, synthetic opals have fcc structure.

[19] K. Ohtaka, Phys. Rev. B **19**, 5057 (1979); W. Lamb, D. M. Wood, and N. W. Ashkroft, Phys. Rev. B **21**, 2248 (1980); X. Wang, X.-G. Zang, Q. Yu, and B. N. Harmon, Phys. Rev. B **47**, 4161 (1992).

[20] N. Stefanou, V. Yannopopas, and A. Modinos, Comput. Phys. Commun. **113**, 49 (1998); N. Stefanou, V. Yannopopas, and A. Modinos, Comput. Phys. Commun. **132**, 189 (2000).

[21] Z. Lin and S. T. Chui, Phys. Rev. E. **69**, 056614 (2004).

[22] A. A. Fedyanin, O. A. Aktsipetrov, D. Kobayashi, K. Nishimura, H. Uchida, and M. Inoue, J. Magn. Magn. Mater. **282**, 256 (2004).

[23] A. G. Zhdanov, A. A. Fedyanin, O. A. Aktsipetrov, D. Kobayashi, H. Uchida, and M. Inoue, J. Magn. Magn. Mater. **300**, e253 (2006).